THREE DIMENSIONAL TURBINE BLADE ANALYSIS IN THERMO-VISCOPLASTICITY

by

M. GÉRADIN (*), J. C. GOLINVAL (*), J. P. MASCARELL (**)

ABSTRACT

Unified elasto-viscoplastic constitutive equation models have been implemented in a general purpose finite element code used in an industrial context for the stressing of structures submitted to high cyclic loading levels. Continuum damage model is used for the lifetime prediction of structures. This paper illustrates the use of these models on a three dimensional turbine blade analysis regarding to the calculations of stress redistributions during the loading cycles and the lifetime prediction. The three dimensional solution is compared to the solution found with the classical uniaxial plane cross-section assumption.

Keywords (NASA thesaurus): Turbine blades – Stress analysis – Lifetime prediction – Model – Non linear equations – Loading cycle.

(*) Professeur, L.T.A.S., Université de Liège (Belgium)..
(**) S.N.E.C.M.A., Centre de Villaroche (France).

I. INTRODUCTION

The lifetime prediction of turbine components submitted to high temperature and to high load level has become a problem of primary importance to aeronautical industries. Higher performance implies higher turbine inlet temperatures and therefore higher service temperature of turbine blades and vanes. Unified viscoplastic models are to be used to compute redistribution of stresses and strains within the part and for the lifetime prediction, S.N.E.C.M.A. uses continuous damage models. These models have been proposed by ONERA for 15 years and the purpose of this paper is to illustrate their use through a 3D finite element analysis regarding to the prediction of stress redistributions, stabilized cycles and lifetime prediction. This paper will present results from calculations conducted on a S.N.E.C.M.A.'s blade thermal fatigue test rig simulating the thermal and centrifugal loadings in sufficiently well known conditions to avoid a large cumulation of uncertainties and approximations.

Unified constitutive models of elasto-viscoplastic material behavior for predicting the response of structures to cyclic loading have been implemented in the general purpose finite element code SAMCEF. They require the time integration of a system of nonlinear first order differential equations. This is done in the code using a variable order, variable time step formulation of the Adams formulas. The resulting algorithm is based on a predictor-corrector method (PECE-method) with self-adaptive time stepping and integration order selection [11].

II. NUMERICAL IMPLEMENTATION

II.1. MECHANICAL BEHAVIOR

The description of the viscoplastic material behavior is based on the unified constitutive models proposed by **Chaboche** [2]. These models are very complete and can be used to describe a large number of phenomena. They applied also to a large variety of materials. The viscoplastic model used for this problem is a five parameter law allowing for the description of non linear kinematic hardening. This model is well suited to the description of stabilized cyclic effects in viscoplasticity. It can be written in the following form:

- *The viscoplastic flow rule*

$$\dot{\boldsymbol{\varepsilon}}^p = \frac{3}{2}\dot{p}\frac{\boldsymbol{\sigma}'-\mathbf{X}'}{J(\boldsymbol{\sigma}'-\mathbf{X}')} \tag{1}$$

with

$$J(\boldsymbol{\sigma}'-\mathbf{X}') = \sqrt{\frac{3}{2}(\boldsymbol{\sigma}'-\mathbf{X}').(\boldsymbol{\sigma}'-\mathbf{X}')}$$

$$\boldsymbol{\sigma}' = \boldsymbol{\sigma} - \frac{1}{3}\mathrm{Tr}(\boldsymbol{\sigma})\,\mathbf{I}$$

$$\mathbf{X}' = \mathbf{X}$$

where

$\dot{\boldsymbol{\varepsilon}}^p$, is the matrix of viscoplastic strain rates;

$\boldsymbol{\sigma}$, is the matrix of deviatoric stresses;

$\dot{p}$, is the accumulated plastic strain rate defined as $\dot{p} = \sqrt{\frac{2}{3}\dot{\boldsymbol{\varepsilon}}^p.\dot{\boldsymbol{\varepsilon}}^p}$;

$\mathbf{I}$, is the unity matrix;

$\mathbf{X}$, is the matrix of internal stresses associated to kinematic hardening.

- *The yield criterion*

$$\dot{p} = \left\langle \frac{J(\boldsymbol{\sigma}'-\mathbf{X}')-k}{K} \right\rangle^n \quad (1) \tag{2}$$

- *The kinematic hardening law*

$$\dot{\boldsymbol{\alpha}} = \dot{\boldsymbol{\varepsilon}}^p - c\,\boldsymbol{\alpha}\,\dot{p} \tag{3}$$

$$\mathbf{X} = \frac{2}{3}ca\,\boldsymbol{\alpha} \tag{4}$$

Equations (2) to (4) involve five material parameters:

- the elastic limit k measures the size of the elastic domain at zero plastic deformation;
- the viscosity parameter K controls the plastic flow rate;
- the viscosity exponent n describes the nonlinearity of the phenomenon;
- the parameter c controls the convergence rate of the model to the stabilized cycle;

(1) $\langle f(x)\rangle = \begin{cases} f(x), \text{ if } f(x)>0; \\ 0, \text{ if } f(x)\leqq 0. \end{cases}$

• the parameter a is the saturation value of $\mathbf{X}$. The product (ca) represents a kinematic hardening modulus.

To take into account the temperature effects on the viscoplastic strain rate, the five material parameters are considered to be temperature dependent. They have been experimentally determined at SNECMA in a large temperature field.

II.2. EQUATIONS OF EQUILIBRIUM

The finite element discretization of the structure based on the Virtual Work Principle within the framework of the total lagrangian formulation leads to the following structural equations of equilibrium:

$$\mathbf{K}\,\mathbf{q} = \mathbf{f} + \mathbf{f}^{p} \tag{5}$$

where

$\mathbf{K}$, is the stiffness matrix;

$\mathbf{q}$, is the vector of nodal displacements;

$\mathbf{f}$, is the vector of equivalent nodal loads;

$\mathbf{f}^{p}$, is the vector of equivalent nodal loads induced by plastic strains.

II.3. TIME INTEGRATION OF THE CONSTITUTIVE EQUATIONS

The model constitutive equations were integrated using a predictor-corrector scheme based on a variable order, variable time step formulation of the Adams formulas:

• *Adams-Bashforth formula of order k used for prediction*

$$\mathbf{Y}_{n+1}^{\text{Pred}} = \mathbf{Y}_{n} + h_{n+1} \sum_{i=1}^{k} a_{k,i}\, \dot{\mathbf{Y}}_{n+1-i}. \tag{6}$$

• *Adams-Moulton formula of order* $(k+1)$ *used for correction*

$$\mathbf{Y}_{n+1}^{\text{Cor}} = \mathbf{Y}_{n} + h_{n+1} \sum_{i=1}^{k} a_{k,i}^{*}\, \dot{\mathbf{Y}}_{n+1-i} + h_{n+1}\, a_{k,0}^{*}\, \dot{\mathbf{Y}}_{n+1}^{\text{Pred}} \tag{7}$$

where

$\mathbf{Y}$, is written as the vector of time-dependent variables *i.e.* the viscoplastic strains and the internal variables;

h_{n+1}, is the time step size;

$a_{k,i}$, $a_{k,i}^{*}$, are a set of coefficients depending on the current order and time step.

The acceptance criterion of the results of a step, the order and time step selection are based on the definition and the estimates of local errors of integration at different times and orders. This results in an efficient algorithm regarding to accuracy, ease of use and computational time even though viscoplastic calculations remain intrinsically expensive. More details on the strategy for selecting the step size and the order and on the implementation of this method in the code SAMCEF were presented in a previous paper [8].

III TURBINE BLADE ANALYSIS

III.1. GEOMETRY

The example considered in this paper is an air-cooled turbine blade designed by SNECMA and used in the high-pressure stage turbine of the LARZAC aircraft engine. The airfoil is about 35.4 mm in span and 24 mm in chord width. The blade is made of a superalloy of type IN 100 incorporating cooling features as shown in Figure 1.

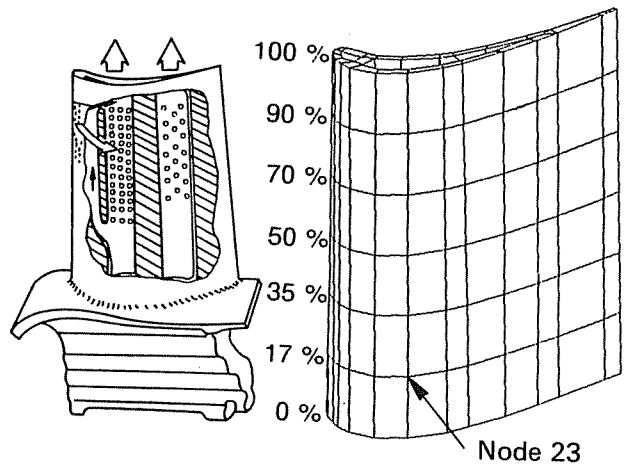

Fig. 1. – Geometry and finite element mesh of the turbine blade.

III.2. LOADING CYCLE

Figure 2 illustrates the centrifugal and thermal loading history of the turbine blade for test rig conditions. The temperature variations on the trailing and leading edges are representative of a typical engine

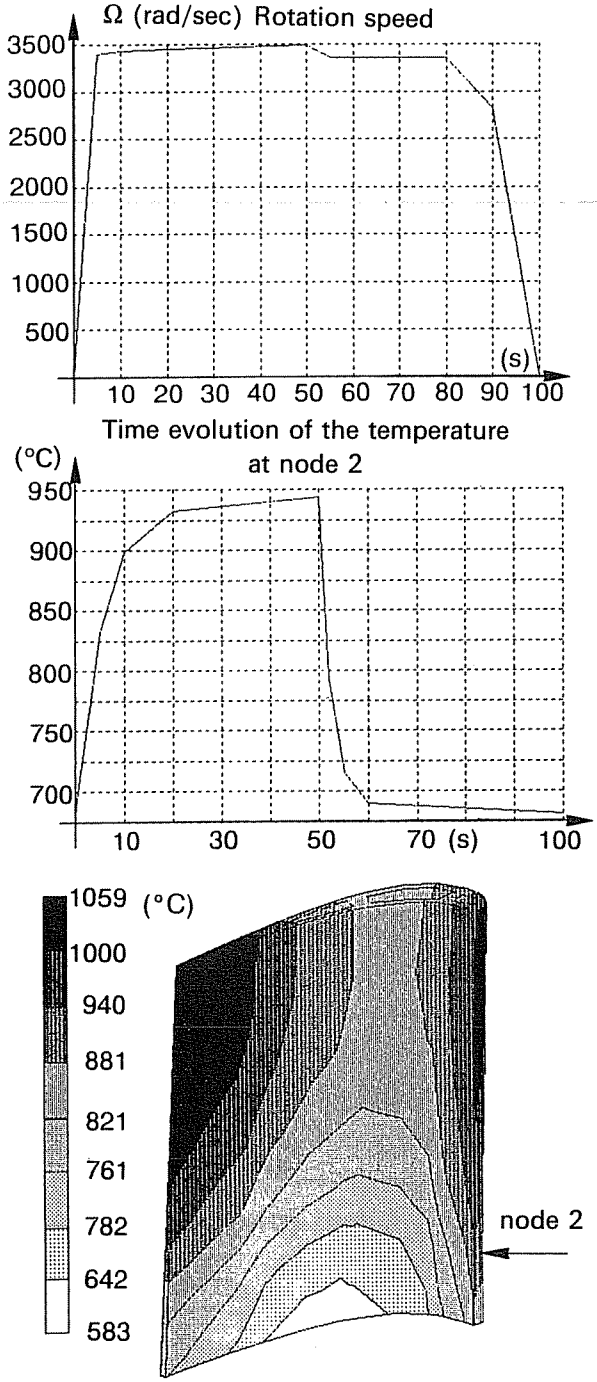

Fig. 2. – Thermal and centrifugal loadind cycle of the turbine blade.

operating cycle; they lead to a fatigue damage due to the repeated successive cycles and to a creep damage due to the long dwell time under high temperature and under centrifugal loads. Temperature distributions in the airfoil were provided by SNECMA at the times given in Figure 2. The temperature distribution is shown at the maximum rotational speed where the highest temperatures occur. The calculated results are consistent with optical pyrometer and thermocouple data in critical zones.

III.3. FINITE ELEMENT DISCRETIZATION

The three-dimensional finite element discretization of the turbine blade is given in Figure 1. The model includes 150 solid 8 node-elements in which the displacement field is quadratic. The blade is divided into 6 rows of 25 cubic elements which give a total amount of 308 nodes and 877 degrees of freedom. All nodes at the base section are constrained to lie on the base plane of the airfoil. Additional boundary conditions were applied to the edge nodes of the base of the blade to prevent rigid body motion.

IV. RESULTS OF THE VISCOPLASTIC CALCULATIONS

Several cyclic viscoplastic calculations of the turbine blade were performed using the finite element code SAMCEF. The calculated radial stress-plastic strain hysteresis loops at the blade lower surface (node 2) of the 17% airfoil section are shown in Figure 3 along with the time evolution of the radial plastic strain. The figure shows the importance of centrifugal stresses that combine with the thermal stresses during the loading rise. For the purpose of this paper, the viscoplastic strain effects were assumed to be small after the fourth cycle so that the fifth cycle is considered as the stabilized cycle.

The CPU time for the first cycle is 6 hours on a Vax Digital 3600 computer and around 3 hours for the following cycles. High transient thermal stresses and viscoplastic strains are induced at the initial time because of non isothermal conditions and during each heating and cooling phase. The accumulated plastic strain distributions are plotted in Figure 4 at the end of the cycle. It is shown that the elements that exhibit the largest viscoplastic strains during the cycle are located at the trailing edge at midspan. Figure 5 gives the corresponding Von Mises effective stress distributions at maximum load levels and at the end of the cycle. During the lower dwell time, the level of effective stresses is high at the leading edge because of the existence of important temperature gradients.

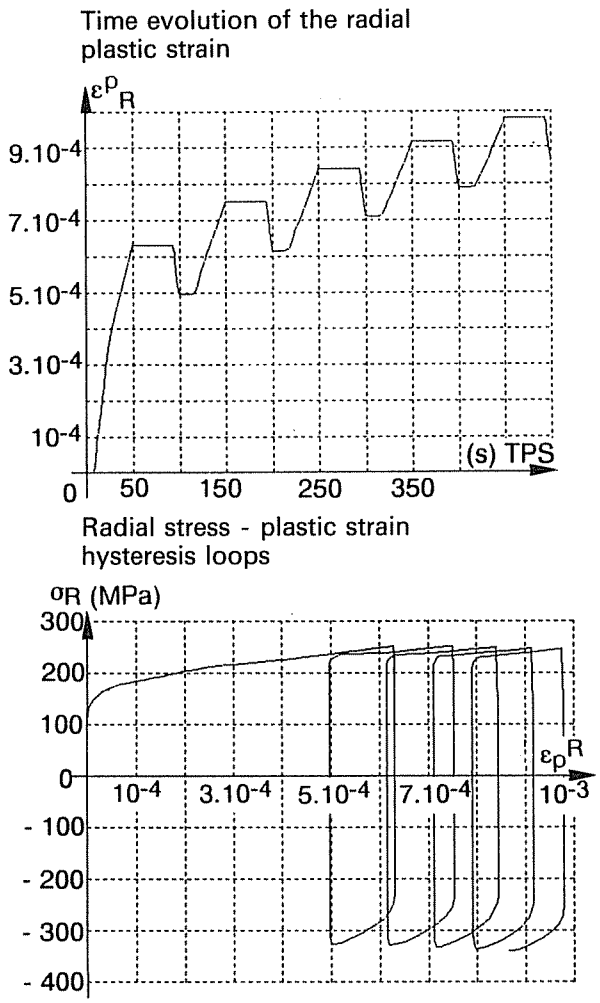

Fig. 3. — Results at node 2.

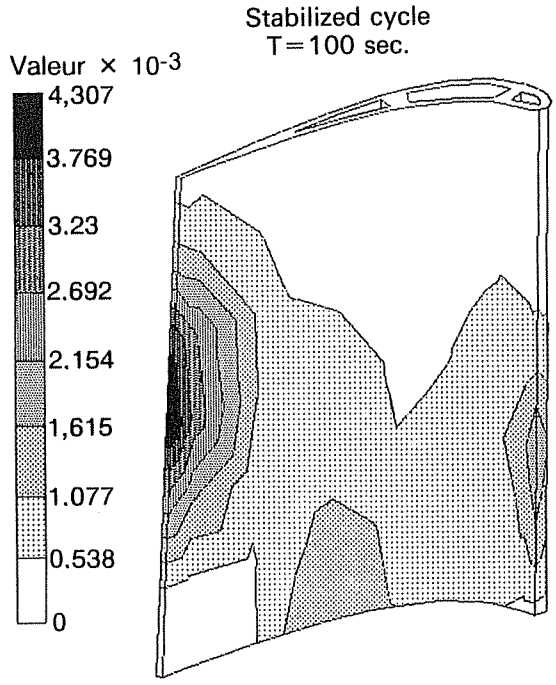

Fig. 4. — Accumulated plastic strain distribution at the end of the stabilized cycle.

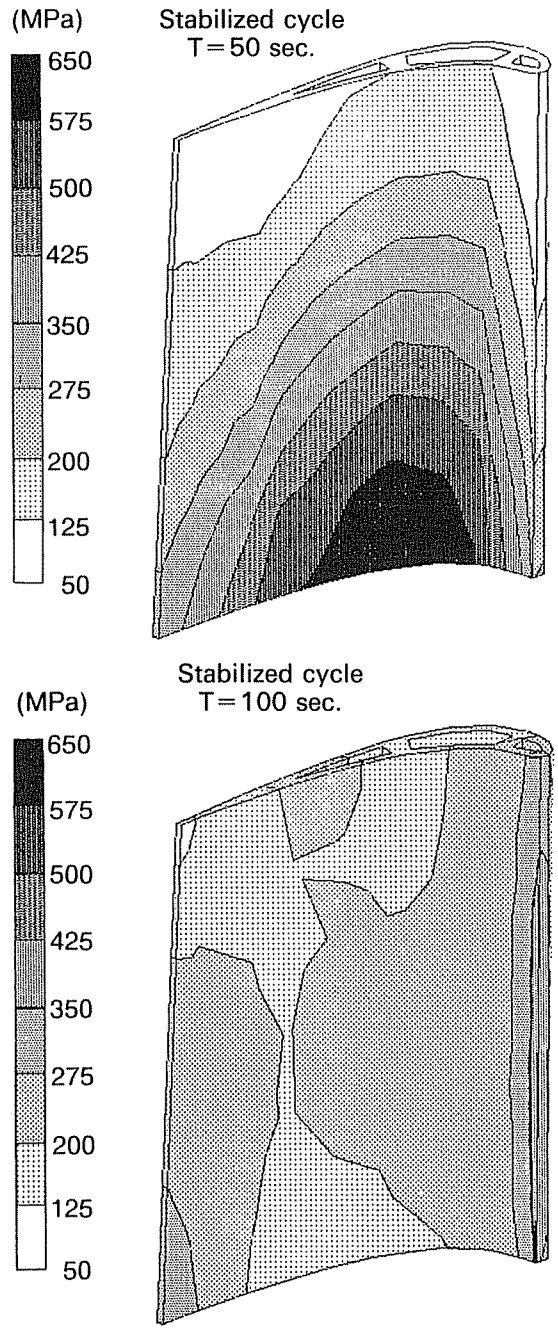

Fig. 5. — Von Mises effective stress distribution at maximal and minimal load levels.

Until recently, viscoplastic and lifetime prediction calculations of turbine blades were conducted using uniaxial models [5]. Calculations were usually done for different airfoil plane sections on the base of the following assumptions:

- two neighbouring cross-sections, initially plane and parallel, remain plane during the deformation process, but may rotate one to each other;

• the Von Mises effective stress is perpendicular to the airfoil section and is equivalent to the radial stress component.

The comparison of the 3D viscoplastic analyses results presented herein with classic uniaxial results is based on the critical test airfoil section at 17%. First a view of displacements on the 50% airfoil section (Fig. 6) shows that the section remains almost plane during the deformation process.

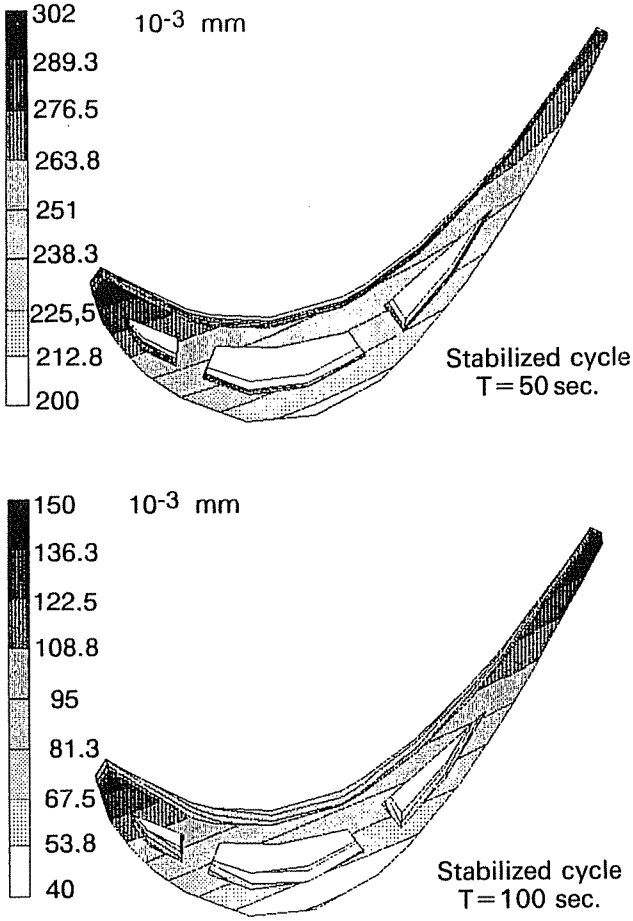

Fig. 6. – Radial displacement distributions on the 50% cross-section
at maximal and minimal load levels.

The time variation of the radial stress component is compared to the Von Mises effective stress at node 23 of the 17% airfoil section along with the uniaxial result (Fig. 7). It can be seen from this figure that the radial stress obtained from the 3D solution is near the uniaxial solution. However, in the present case, the radial stress component appear to be significantly lower than the Von Mises effective stress. This indicates that the stress triaxiality is significant in this part. For this example, the 3D calculation agrees approximately with the plane cross-section assumption and brings additional information on the stress distribution, although the accuracy of the 2D model might be sufficient in many cases.

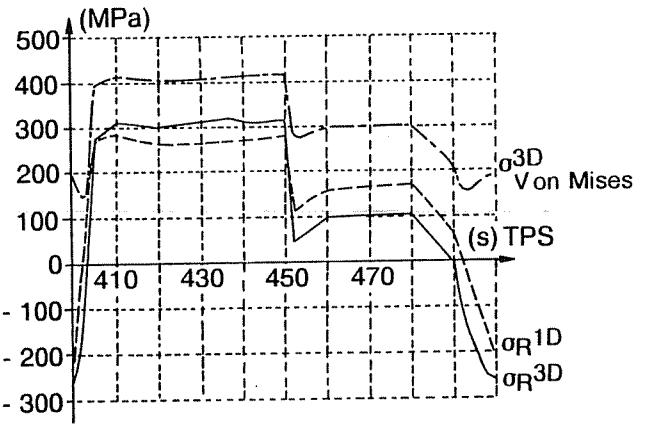

Fig. 7. – Comparison of the radial stress component and of the Von Mises effective stress at node 23.

V. LIFETIME PREDICTION

The fatigue and creep damage can be calculated from the history of stresses, strains and temperatures. Since the two processes interact at high temperature,

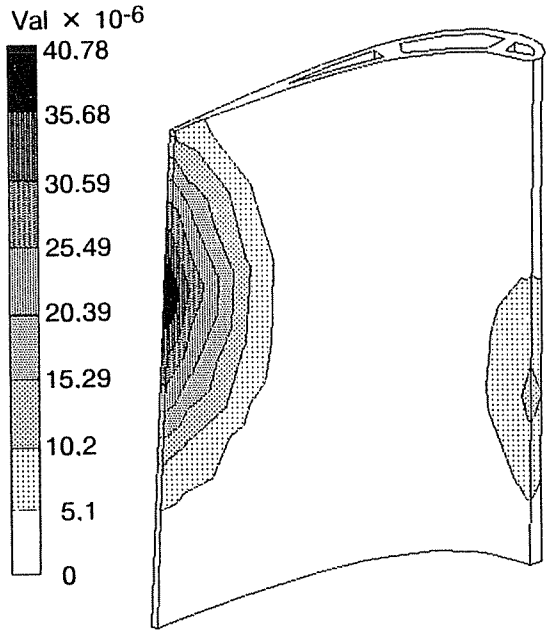

Fig. 8. – Accumulated creep damage distribution at the end of the stabilized cycle.

the two effects are cumulative. The pure fatigue lifetime is predicted using a criterion dependent on the maximum and average stress levels but it appears to be negligible in the present analysis. The creep damage law is the Kachanov law assuming a different damage in the traction and compression modes. It can be written as follows:

$$\dot{D} = \left\langle \frac{\chi(\sigma)}{A} \right\rangle^{r} (1-D)^{r-k} \qquad (8)$$

where

D, is the creep damage variable;

χ, is a stress measure combining the first three stress invariants;

A, r, k, are temperature dependent parameters.

The accumulated creep damage distribution for the stabilized cycle is shown in Figure 8. The critical blade zones were found to agree the uniaxial prediction.

VI. CONCLUSIONS

The present analysis demonstrates the ability of 3D finite element codes to modelize complex structures under high cyclic load levels using unified constitutive equations. These calculation methods are implemented in the general purpose finite element code SAMCEF used by SNECMA for aircraft engine stressing. For blades made of an isotropic polycristalline superalloy, the 3D calculation agrees with the uniaxial models but these last ones would be inadequate for single cristal analyses or local stress studies.

Manuscript submitted February 28, 1989.

REFERENCES

[1] BOUCHERIT A. et MASCARELL J. P. – *Dimensionnement à chaud des disques de turbomachines,* Bulletin S.F.M., Revue Française de Mécanique, n° 1988-1.

[2] CHABOCHE J. L. – *Description thermodynamique et phénoménologique de la viscoplasticité cyclique avec endommagement,* Thèse, Publication ONERA, 1978-3.

[3] CHABOCHE J. L. – *Stress calculations for lifetime prediction in turbine blades,* Int. J. Solids Structures, vol. 10, (1974), p. 473-481.

[4] CHABOCHE J. L. et CULIE J. P. – *On turbine blade creep and fatigue analysis by special kinematic assumptions,* Intern. Conf. on Engineering Aspects of Creep, Sheffield, G.-B., 15-19 septembre, (1980).

[5] CHABOCHE J. L. et STOLTZ. – *Détermination des durées de vie des aubes de turbine à gaz,* Revue Française de Mécanique, n° 52, (1974), p. 37-47.

[6] DAMBRINE B. et MASCARELL J. P. – *About the interest of using unified viscoplastic models in engine hot components life prediction,* Intern. Sem. on High Temperature Fracture Mechanisms and Mechanics, Dourdan, France, (1987).

[7] GEAR C. W. – *Numerical initial value problems in ordinary differential equations,* Prentice-Hall, Englewood Cliffs, N.J., (1971).

[8] GOLINVAL J. C. et GÉRADIN M. – *Implementation of thermo-viscoplastic constitutive equations into the finite element code SAMCEF for the response of structures to cyclic loading,* Intern. Sem. on High Temperature Fracture Mechanisms and Mechanics, Dourdan, France, (1987).

[9] KAUFMAN A., TONG M., SALTSMAN J. F. et HALFORD G. R. – *Structural analysis of turbine blades using unified constitutive models,* IMechE 1987 CO 4/87.

[10] LEMAITRE J. et CHABOCHE J. L. – Mécanique des matériaux solides, Dunod, Paris, (1985).

[11] SAMCEF, Module de réponse en viscoplasticité cyclique : VISCO, LTAS, (1988).

[12] SHAMPINE L. F. et GORDON M. K. – *Computer solution of ordinary differential equations: the initial value problem,* W.H. Freeman and Company, (1975).